Development of a Salted Extended Kalman Filter for the Hybrid-Dynamic Walking of a Bipedal Robot

Ashutosh Mukherjee, Institute of Engineering Mechanics, Karlsruhe Institute of Technology, Karlsruhe;
Yinnan Luo, Institute of Engineering Mechanics, Karlsruhe Institute of Technology, Karlsruhe;
Max Horst Bauer, Institute of Engineering Mechanics, Karlsruhe Institute of Technology, Karlsruhe;
Marten Zirkel, Mechanics of Compliant Systems Group, TU Ilmenau, Ilmenau;
Erik Gerlach, Mechanics of Compliant Systems Group, TU Ilmenau, Ilmenau;
Lena Zentner, Mechanics of Compliant Systems Group, TU Ilmenau, Ilmenau;
Alexander Fidlin, Institute of Engineering Mechanics, Karlsruhe Institute of Technology, Karlsruhe

Abstract

Accurate state estimation is critical for the controller design of bipedal robots such as the Hybrid Zero-Dynamics approach. This work investigates a Salted Extended Kalman Filter (SEKF), an EKF variant for hybrid dynamics, within a real-time simulation of a planar five-link robot model. Measurement noise characteristics are identified from encoder data from a real robot prototype and the SEKF is tested under both actual and augmented noise parameters. The SEKF demonstrates reliable state estimation across impacts, effective noise suppression, and facilitates controller performance, and necessary extensions for deployment on a physical prototype are presented.

1. Introduction

Recent research in bipedal robotics has focused on stable, energy-efficient locomotion. Notable examples include RABBIT and ERNIE [1, Ch. 1], point-foot bipeds used as testbeds for developing advanced control algorithms allowing stable locomotion making use of the passive dynamics of the legs; MABEL [2] and WALK-MAN [3], bipeds with compliant drivetrains to improve efficiency; and WANDERER [4], a robot with passive joint mechanisms for long-duration walking, to name a few. At the Karlsruhe Institute of Technology's Institute of Engineering Mechanics, similar efforts have been carried out in generating energy-efficient walking and running gaits for point-foot bipeds with elastic couplings [5,6]. To experimentally validate the existing simulation results in laboratory conditions, a bipedal robot prototype, operating under the Hybrid-Zero Dynamics approach presented in [1, Ch. 6] has been constructed for real-time walking tests. For such a complex mechatronic system, accurate and robust control hinges on sensor quality. Although low-pass filtering, a traditional solution, can suppress measurement noise effectively, it also introduces time-delay, necessitating a trade-off between filtering strength and stability margins. Hence, various forms of Kalman Filtering have become a popular choice for mobile robotics, especially the Extended Kalman Filter

(EKFs) for on-board applications, thanks to the reasonable balance between on-board computational ability and accuracy. Apart from filtering out noise within the system, EKFs also facilitate multi-sensor fusion, where measurement data from variety of sensor sources can be combined together to make the estimation of system states more robust. However, there is a special feature of bipedal robots that traditional EKFs are not equipped to handle: bipedal walking is inherently a hybrid dynamical system, while EKFs are designed to only handle continuous dynamics. There have been several approaches to tackle this challenge, with the one of the latest methods being the usage of Saltation Matrices [7], to accommodate the change in dynamics across hybrid transitions of walking in the EKF, the so-called Salted Extended Kalman Filter (SEKF) [8]. In this paper, the primary implementation of the SEKF for the system of the bipedal robot in a real-time simulation framework is presented, wherein the quality of state-estimation for hybrid dynamical walking in comparison to a traditional EKF is investigated and subsequently the feasibility for deployment on the bipedal robot prototype is discussed.

1.1 Related Works and State of the Art

In the recent years, Kalman filtering has found a lot of use in mobile robotics. In [9] an observability constrained EKF framework for a quadruped platform is introduced, where kinematic encoder data is fused with on-board Inertial Measurement Unit (IMU) measurements. By propagating the estimates via strapdown equations, the complex dynamic model of the quadruped was avoided, while measurement correction from kinematic foot data enabled robust performance across terrains and gaits. A similar contact-aided structure was implemented for the MIT Cheetah 3 in [10], where IMU-based dead reckoning was corrected using encoder data. Through this two-stage framework, the second stage can be formulated as a linear process, which allows use of linear Kalman Filter, guaranteeing filter convergence. The approach was later extended in [11] by combining contact-aided filtering with invariant Kalman filtering [12], leveraging Lie group symmetries of the resulting system to achieve log-linear error dynamics independent of current estimates and improved convergence, and validated in both simulation and experiments for bipeds. However, these works did not account for the hybrid nature of bipedal locomotion. The Salted EKF (SEKF) [8], addresses this by incorporating the Saltation Matrix to approximate error dynamics across discrete transitions, updating covariances at each impact. The SEKF is shown to have comparable performance with a hybrid particle filter up until a high number of particles, at which point in any case the use of particle filters for on-board applications becomes unfeasible. In spite of its promising performance, the SEKF struggles with the usual convergence issues of an EKF and is strongly dependent on decent filter initializations. Extensions were proposed in [13] to account for transition uncertainties, and later combined with invariant Kalman filtering in [14] to form the Hybrid Invariant EKF, evaluated for bipeds on dynamic rigid surfaces. Apart from EKFs, filters

more suited for highly non-linear systems can also be found in the literature, for instance the hybrid Unscented Kalman Filter (UKF), but given real-time feasibility constraints, the EKF remains preferable., and since currently the prototype is currently not equipped with IMUs, the invariant Kalman filter structure can't be exploited, making SEKF the filter of choice.

1.2 Structure of the Paper

The structure of the following paper is as follows: The Bipedal Robot Prototype and its reduced mechanical model along with the underlying principles of Bipedal Walking are introduced in Section 2, Hybrid-Zero Dynamics Control is discussed briefly in Section 3, the SEKF is introduced in Section 4, with the integration of the filter within the closed-loop system of the robot being elaborated in Section 5. The primary simulation results are discussed in Section 6, and the conclusion of the study and future outlook are given in Section 7.

2. Bipedal Walking System

2.1 Bipedal Robot Prototype

The side and front profiles of the Bipedal Robot Prototype, which has been developed at the Institute of Engineering Mechanics to carry out the walking experiments, is shown in Figure 1.

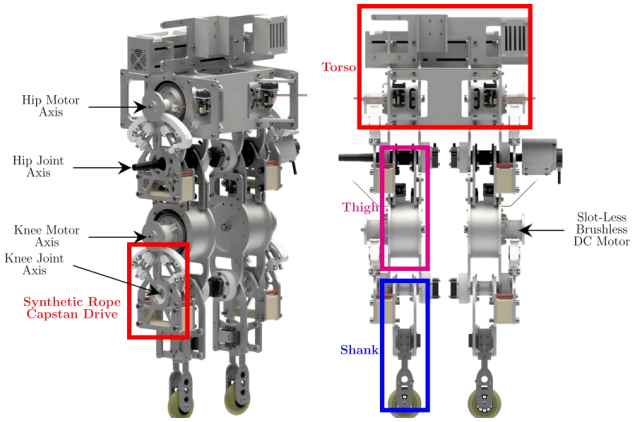

Figure 1: Side (left) and Front (right) profiles of the Robot Prototype without cabling or electronics

The prototype consists of five rigid segments: two thighs, two shanks and one torso. The prototype is actuated at each of its four joints in the legs, two hips and two knees, using slot-less brushless DC motors from *Celera Motion.* To accommodate high torque values

required during bipedal walking, synthetic rope based Capstan Drives [15] are used to transmit the torques from each motor to their respective joints. To simplify the model of the prototype for simulations, a reduced mechanical model of the robot is assumed, shown in Figure 2. In this model, the entire drivetrain is reduced to the corresponding joints, naturally assuming rigid connections. This reduced model facilitates not just the previous simulation studies, but also the validation of the filter design. The various mechanical parameters of the reduced model given by $\boldsymbol{p} \in \mathbb{R}^{13}$ were identified using a framework, which can be referred from [16].

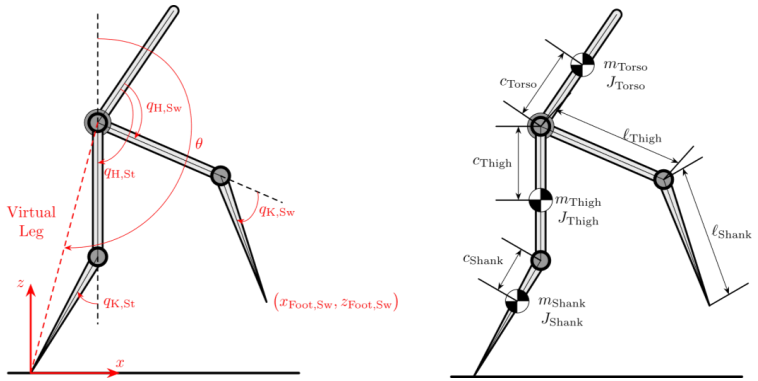

Figure 2: Reduced Mathematical Model of Robot with Generalized Coordinates (Left) and Mechanical Parameters (Right)

2.2 Modeling of Planar Bipedal Robot with Point Feet

The reduced mechanical model is used to describe the robot's planar bipedal walking in the sagittal plane, following the formulation in [1, Ch. 3]. Both legs contact the flat rigid ground through the point foot i.e. no foot segments or ankle joints are considered. The walking is modelled as a periodic sequence of the continuous *Single Support Phase (SSP)*, wherein the entire robot propels further about the point contact between the ground and the stance leg, and the instantaneous and discrete *Double Support Phase (DSP),* wherein the swing leg impacts the ground and the stance leg lifts off the ground.

2.2.1 Continuous Single Support Phase (SSP)

During SSP, the robot is assumed to be a pinned open kinematic chain, with the stance leg point foot acting as an ideal pivot without any slipping. The generalized coordinates of the robot are formulated as $\boldsymbol{q} = (\theta \quad q_{\mathrm{H,St}} \quad q_{\mathrm{H,Sw}} \quad q_{\mathrm{K,St}} \quad q_{\mathrm{K,Sw}})^{\mathrm{T}} = \left(\theta \quad \boldsymbol{q}_J{}^{\mathrm{T}}\right)^{\mathrm{T}} \in \mathcal{Q}_S$ where $\mathcal{Q}_S$ is the five-dimensional configuration space of the robot and θ describes the absolute angle of the virtual leg, which is the straight line connecting the hip joint and the point contact of the stance

leg, as shown in Figure 2. $q_{\mathrm{H,St}}, q_{\mathrm{H,Sw}}, q_{\mathrm{K,St}}, q_{\mathrm{K,Sw}}$ describe the relative angles between the segments. The non-linear state-space representation with the state vector $\boldsymbol{x} = (\boldsymbol{q}, \dot{\boldsymbol{q}})^{\mathrm{T}} \in TQ_S \subseteq \mathbb{R}^{10}$ is given by $\dot{\boldsymbol{x}} = \tilde{\boldsymbol{f}}(\boldsymbol{x}) + \tilde{\boldsymbol{g}}(\boldsymbol{x})\boldsymbol{u}$ where $\boldsymbol{u} \in \mathbb{R}^4$ is the vector of applied joint torques.

2.2.2 Discrete Impact Model (DSP)

During the discrete DSP, the generalized coordinates remain unchanged while the generalized velocities need to be updated, which is carried out by assuming an inelastic contact with the ground and solving the linear and angular momentum balance equations at impact. Subsequently, the pre-impact states $(\boldsymbol{x})$ are updated to the post-impact states $(\tilde{\boldsymbol{x}})$ using the derived reset map. The order of swing and stance legs is always maintained in the state and generalized quantities vectors, which facilitates the re-use of the same SSP dynamics post-impact, due to which a coordinate switch transformation is carried out, through which the legs switch their roles after each impact. The final post-impact states are given by

$$\tilde{\boldsymbol{x}} = \boldsymbol{\Delta}(\boldsymbol{x}) \tag{1}$$

Details about deriving the final impact map $\boldsymbol{\Delta}(\boldsymbol{x})$ can be referred from [12, Ch. 3].

2.2.3 Hybrid Model of Walking

The continuous SSP and discrete DSP are stitched together periodically to obtain the hybrid model of bipedal walking given by

$$\Sigma_{\mathrm{Walking}}: \begin{cases} \dot{\boldsymbol{x}} = \tilde{\boldsymbol{f}}(\boldsymbol{x}) + \tilde{\boldsymbol{g}}(\boldsymbol{x})\boldsymbol{u}, \boldsymbol{x} \notin \mathcal{G} \\ \tilde{\boldsymbol{x}} = \boldsymbol{\Delta}(\boldsymbol{x}), \boldsymbol{x} \in \mathcal{G} \end{cases} \tag{2}$$

$\mathcal{G}$ represents the switching set given by

$$\mathcal{G} := \{ \boldsymbol{x} \in TQ_S \mid z_{\mathrm{Foot,Sw}} = 0, x_{\mathrm{Foot,Sw}} = l_{\mathrm{Step}} \} \tag{3}$$

where $\boldsymbol{r}_{\mathrm{Foot,Sw}} = (x_{\mathrm{Foot,Sw}} \quad z_{\mathrm{Foot,Sw}})^{\mathrm{T}}$ represents the cartesian position of the swing leg foot with respect to the coordinate system originating at the stance leg point contact, as shown in Figure 2 and l_{Step} is the step-length. Essentially, impact switch is carried out only when the height of the swing foot from the ground is negligible and the foot is a walking step-length away from the stance leg. The new post-impact states $(\tilde{\boldsymbol{x}})$ then act as the initial conditions for the next phase of continuous SSP.

3. Hybrid Zero Dynamics Control

The primary objective of Hybrid Zero Dynamics (HZD) Control is to generate stable and periodic walking and running gaits for a bipedal robot, wherein all actuated joints are aligned to the Virtual Angle θ via so-called *Virtual Constraints*. The reference trajectory is subsequently set as a higher-order polynomial defined in terms of the virtual leg angle. Once synchronization is achieved, the dynamics of the full-order bipedal robot are reduced to the Zero-Dynamics submanifold, which is invariant to feedback control and of a lower order. If the reduced zero-dynamics system evolves as a stable limit cycle, a stable walking gait is guaranteed for the

full-order bipedal robot. Theoretical details of HZD can be referred to from [1, Ch. 6]. In the upcoming sections, the ideal closed loop simulation model of the Bipedal Robot with HZD Control and without any noise or filter implementation is referred to as *Ground Truth.*

4. EKF and SEKF in discrete time

In this work, the implementation of the Extended Kalman Filter in discrete time is used. Since the extended Kalman Filter in discrete time is already thoroughly covered in literature, it won't be introduced in detail in this work. For details on the discrete EKF, readers can refer to various sources like [17]. Within the SEKF, the state estimates and the estimate covariance matrix are updated over the discrete transition with the help of the reset-map and the Saltation Matrix respectively. The Saltation Matrix $\boldsymbol{\Xi}$ is a linear approximation of the variances and covariances about the nominal trajectory i.e. the current state estimate across the discrete transition [8, 18]. In this work, the a-priori state and covariance estimates (before the measurement update at time-step k) are denoted as $\hat{\boldsymbol{x}}_k^-, \hat{\boldsymbol{P}}_k^-$ and the a-posteriori estimates (after the update) as $\hat{\boldsymbol{x}}_k^+, \hat{\boldsymbol{P}}_k^+$. The discrete transition is assumed to always take place at the start of the filter time-step, followed by the propagation and the measurement correction steps. Thus, the pre-transition values are the a-posteriori estimates from the previous step $\hat{\boldsymbol{x}}_{k-1}^+, \hat{\boldsymbol{P}}_{k-1}^+$ while the post-transition quantities are denoted as $\tilde{\boldsymbol{x}}_k^-, \tilde{\boldsymbol{P}}_k^-$. A hat on top denotes that it is an estimation in continuous domain, a tilde on top denotes an estimation post-impact, and absence of either denotes that it is a true value.

4.1 Guard Function and Saltation Matrix

For the robot, the pre- (I) and post-continuous (J) domains are identical except for the coordinate switch. The discrete transition is triggered on the basis of the guard function vector $\boldsymbol{g}_{IJ}(\hat{\boldsymbol{x}}_{k-1}^+) \in \mathbb{R}^2$ and given by

$$\boldsymbol{g}_{IJ}(\hat{\boldsymbol{x}}_{k-1}^+) = (g_1 \quad g_2)^\intercal = (r^x_{\mathrm{Foot,Sw}} - l_{\mathrm{Step}} \quad r^z_{\mathrm{Foot,Sw}})^\intercal \tag{4}$$

The impact update is executed only if the corresponding transversality conditions [6] are met, otherwise *grazing* (when $\dot{\boldsymbol{g}}_{IJ} \approx \boldsymbol{0}$) or *multiple* impacts (when $\dot{\boldsymbol{g}}_{IJ} > \boldsymbol{0}$) are assumed and the update is abandoned. Let the continuous vector fields within domains I and J be $\boldsymbol{f}_I$ and $\boldsymbol{f}_J$ respectively. Then, the Saltation Matrix $\boldsymbol{\Xi}_{IJ} \in \mathbb{R}^{10\times10}$ is given by

$$\begin{aligned}\boldsymbol{\Xi}_{IJ} = {} & \nabla_x \boldsymbol{\Delta}_{IJ}(\hat{\boldsymbol{x}}_{k-1}^+) \\ & + \big(\boldsymbol{f}_J(\tilde{\boldsymbol{x}}_k^-) \\ & - \nabla_x \boldsymbol{\Delta}_{IJ}(\hat{\boldsymbol{x}}_{k-1}^+)\boldsymbol{f}_I(\hat{\boldsymbol{x}}_{k-1}^+)\big)\big(\nabla_x \boldsymbol{g}_{IJ}(\hat{\boldsymbol{x}}_{k-1}^+)\boldsymbol{f}_I(\hat{\boldsymbol{x}}_{k-1}^+)\big)^\dagger \nabla_x \boldsymbol{g}_{IJ}(\hat{\boldsymbol{x}}_{k-1}^+)\end{aligned} \tag{6}$$

where $\left(\nabla_x \boldsymbol{g}_{IJ}(\widehat{\boldsymbol{x}}_{k-1}^+)\boldsymbol{f}_I(\widehat{\boldsymbol{x}}_{k-1}^+)\right)^\dagger \in \mathbb{R}^{1\times 2}$ is a pseudo-inverse of the guard-function time-derivative. For a clean numerical implementation of the Saltation Matrix, the reset map and the

Algorithm: Salted Extended Kalman Filter for Bipedal Robot

Input : $\boldsymbol{p}, l_{\text{Step}}, z_{\text{Tol}}, \boldsymbol{\Delta}_{IJ}, \boldsymbol{g} = (\ g_1 \quad g_2\ )^\intercal, \Delta t, N, \boldsymbol{Q}_k, \boldsymbol{R}_k, \hat{\boldsymbol{x}}_0, \hat{\boldsymbol{P}}_0$
Output: $\{\hat{\boldsymbol{x}}_k^+, \hat{\boldsymbol{P}}_k^+\}_{k=N}$
$\hat{\boldsymbol{x}}_0^+ \leftarrow \hat{\boldsymbol{x}}_0,\ \hat{\boldsymbol{P}}_0^+ \leftarrow \hat{\boldsymbol{P}}_0$ `// Initialize State Vector and Covariance Matrix`

for $k \leftarrow 1$ **to** N **do**
  `// Check for Impacts`
  if $g_2(\hat{\boldsymbol{x}}_{k-1}^+) \le z_{\text{Tol}}$ **and** $g_1(\hat{\boldsymbol{x}}_{k-1}^+) \ge \frac{l_{\text{Step}}}{2}$ **and** $(\nabla_t \boldsymbol{g} + \nabla_x \boldsymbol{g}\boldsymbol{f}_I) < \boldsymbol{0}$ **then**
    `// Impact Detected`
    Update $\tilde{\boldsymbol{x}}_k^- \leftarrow \boldsymbol{\Delta}_{IJ}(\hat{\boldsymbol{x}}_{k-1}^+, t_{k-1})$
    Compute $\boldsymbol{\Xi}_{IJ} \leftarrow \nabla_x \boldsymbol{\Delta}_{IJ} + (\boldsymbol{f}_J - \nabla_x \boldsymbol{\Delta}_{IJ}\boldsymbol{f}_I - \nabla_t \boldsymbol{\Delta}_{IJ})(\nabla_t \boldsymbol{g} + \nabla_x \boldsymbol{g}\boldsymbol{f}_I)^\dagger \nabla_x \boldsymbol{g}$
    Update $\tilde{\boldsymbol{P}}_k^- \leftarrow \boldsymbol{\Xi}_{IJ}\, \hat{\boldsymbol{P}}_{k-1}^+\, \boldsymbol{\Xi}_{IJ}^\top$
  else
    `// No Impact Update`
    $\tilde{\boldsymbol{x}}_k^- \leftarrow \hat{\boldsymbol{x}}_{k-1}^+,\ \tilde{\boldsymbol{P}}_k^- \leftarrow \hat{\boldsymbol{P}}_{k-1}^+$
  `// Propagation`
  Update $\hat{\boldsymbol{x}}_k^- \leftarrow \boldsymbol{f}(\tilde{\boldsymbol{x}}_k^-, \boldsymbol{u}_{k-1}, t_{k-1})$
  Compute $\boldsymbol{\Phi}_k \leftarrow \nabla_x \boldsymbol{f}|_{(\tilde{\boldsymbol{x}}_k^-, \boldsymbol{u}_{k-1}, t_{k-1})}$
  Update $\hat{\boldsymbol{P}}_k^- \leftarrow \boldsymbol{\Phi}_k\, \tilde{\boldsymbol{P}}_k^-\, \boldsymbol{\Phi}_k^\top + \boldsymbol{Q}_k$
  if $\boldsymbol{y}_k^{\text{meas}}$ present **then**
    `// Correction`
    $\boldsymbol{C}_k \leftarrow \nabla_x \boldsymbol{c}|_{\hat{\boldsymbol{x}}_k^-}$
    $\boldsymbol{K}_k \leftarrow \hat{\boldsymbol{P}}_k^- \boldsymbol{C}_k^\top \left(\boldsymbol{C}_k \hat{\boldsymbol{P}}_k^- \boldsymbol{C}_k^\top + \boldsymbol{R}_k\right)^{-1}$
    $\hat{\boldsymbol{x}}_k^+ \leftarrow \hat{\boldsymbol{x}}_k^- + \boldsymbol{K}_k\left(\boldsymbol{y}_k^{\text{meas}} - \boldsymbol{c}(\hat{\boldsymbol{x}}_k^-)\right)$
    $\hat{\boldsymbol{P}}_k^+ \leftarrow \hat{\boldsymbol{P}}_k^- - \boldsymbol{K}_k \boldsymbol{C}_k \hat{\boldsymbol{P}}_k^-$
  else
    $\hat{\boldsymbol{x}}_k^+ \leftarrow \hat{\boldsymbol{x}}_k^-,\ \hat{\boldsymbol{P}}_k^+ \leftarrow \hat{\boldsymbol{P}}_k^-$
return $\{(\hat{\boldsymbol{x}}_k^+, \hat{\boldsymbol{P}}_k^+)\}_{k=N}$

Algorithm 1: SEKF Algorithm

guard function should be differentiable. Within the framework of the SEKF, the discrete transition updates to the state-estimates and the estimate covariance matrix are given by

$$\widetilde{\boldsymbol{x}}_k^- = \boldsymbol{\Delta}_{IJ}(\widehat{\boldsymbol{x}}_{k-1}^+) \tag{5}$$

$$\widetilde{\boldsymbol{P}}_k^- = \boldsymbol{\Xi}_{IJ}\widehat{\boldsymbol{P}}_{k-1}^+\boldsymbol{\Xi}_{IJ}^\intercal \tag{6}$$

Theoretical details of the Saltation Matrix can be referred to from [8,18].

5. Implementation of SEKF for Bipedal Walking

5.1 SEKF Algorithm

Algorithm 1 illustrates the algorithm of the SEKF for the Bipedal Robot. Important initializations for the algorithm include: the initial state estimate and covariance matrix $\widehat{\boldsymbol{x}}_0, \widehat{\boldsymbol{P}}_0$, the process and measurement noise matrices $\boldsymbol{Q}_k, \boldsymbol{R}_k$, the desired step-length for walking l_{Step}, the guard functions and the impact reset map, the filter step-size Δt and all relevant mechanical parameters of the reduced mechanical model $\boldsymbol{p}$.

5.2 Integrated Closed-Loop

Figure 3 illustrates the closed-loop architecture of the Bipedal Robot with the integrated SEKF. The states of the Bipedal Robot are corrupted using artificial sensor noise, to emulate real sensor measurements. The relevant angles and their corresponding velocities in the prototype are measured with the help of absolute encoders, which means the measured quantities $\boldsymbol{y}^{\text{meas}}$ are just corrupted versions of the actual robot states. One of the fundamental assumptions of a Kalman Filter is that the measurement noise is a zero-mean gaussian white noise, hence the corrupted states are just signals normally distributed about the actual states with variance $\delta\boldsymbol{x}$ i.e. $\boldsymbol{y}^{\text{meas}} = \mathcal{N}(\boldsymbol{x}, \delta\boldsymbol{x})$. The corrupted states are then fed to the SEKF, which estimates the states and feeds it forward to the feedback controller.

5.3 Sensor Noise

Given the zero-mean gaussian white-noise assumption in a Kalman Filter, it is prudent to investigate the behavior of the sensors being used for the prototype. Currently, the relative angles between the segments $(\boldsymbol{q}_J)$ are measured using *IncOder Inductive* Angle Encoders (motor encoders), model INC-3-100, with 21 bits resolution while the *Novohall RFC-4800 SPI Encoder* (Hip Encoder) from *Novotechnik* with 14 bits resolution is used to measure the absolute angle of the stance leg thigh with respect to the environment, from which the virtual leg angle measurement can be computed. Stationary measurements from both encoders is recorded and their corresponding noise distributions have been illustrated in Figure 4.

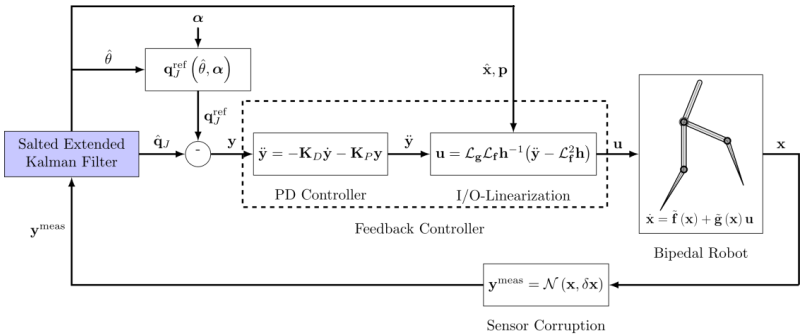

Figure 3: Closed Loop Architecture for Bipedal Robot with SEKF

It is quite clear that none of the measurements are purely gaussian in nature, with the motor encoder angles seeming to be uniformly distributed, motor encoder velocities seemingly being noise-free, the hip-encoder angles being heavily quantized due to the lower bit resolution and the hip encoder velocity measurements seeming to be multi-modal in nature. The non-

gaussian nature of the encoder measurements can be attributed as a possible source of error for the filter performance. Using a gaussian fit, the variances of each measurements are computed to be

$$\sigma^2 = \{5.6 \times 10^{-8} \quad 1.3 \times 10^{-8}\mathbf{I}_{1\times4} \quad 5.9 \times 10^{-4} \quad \mathbf{0}_{1\times4}\}$$

5.4 Parameter Tuning

The measurement and process covariance matrices $\boldsymbol{R}_k, \boldsymbol{Q}_k$ and the initial error covariance matrix $\boldsymbol{P}_0$ need to be tuned for obtaining optimal filter performance. The measurement covariance is set exactly as the evaluated covariances from the gaussian fits of the encoder data. The process noise is primarily expected from the deviation between the control plant i.e. the Bipedal Robot simulation model, where the forward dynamics are solved using 4th-Order Runge-Kutta Integrator and the state transition matrix in the propagation step of the filter, which is obtained from a simple Euler Integration of the equations of motion. The process covariance is set as $\boldsymbol{Q}_k = 1 \times 10^{-4}\boldsymbol{I}_{10\times10}$, while the initial covariance matrix is set as $\boldsymbol{P}_0 = 1 \times 10^{-6}\boldsymbol{I}_{10\times10}$. For the above parameter values, the SEKF converges, but optimal performance can't be guaranteed. While standard tuning procedures for the filter don't exist, strategies like grid-search or even Adaptive Kalman Filters [19], where the noise covariance matrices are updated based on current estimates, can be implemented.

5.5 Comparison against a traditional EKF

To elucidate the advantages of incorporating the Saltation Matrix within the EKF, the performance of the SEKF is compared against that of a traditional EKF, wherein the linearized change in the error variances over the discrete impact is assumed to be represented by the Jacobian of the reset-map $\boldsymbol{\Delta}_{IJ}$. Hence, for the traditional EKF, the covariance matrix update will be given by

$$\widetilde{\boldsymbol{P}}_k^- = \nabla_x \boldsymbol{\Delta}_{IJ}(\widehat{\boldsymbol{x}}_{k-1}^+)\widehat{\boldsymbol{P}}_{k-1}^+ \nabla_x \boldsymbol{\Delta}_{IJ}^{\mathsf{T}}(\widehat{\boldsymbol{x}}_{k-1}^+)$$

This representation, while intuitive in the context of an EKF, usually fails to capture the effective change in the error variances in event-driven hybrid systems [18].

5.6 Real-Time Simulation

To test the real-time capability of the SEKF, the simulation framework for the closed-loop system illustrated in Figure 3 is built in a Real-Time Simulation environment, using a *Speedgoat Baseline Real-Time* target machine that runs the system with a sampling rate of one millisecond. Since the motor and hip encoders communicate with the controller with a sampling time of two milliseconds on the prototype, the measurement correction rate within the SEKF is also set as two milliseconds i.e. every alternate time-step. The reference trajectory for the feedback controller is generated from an offline optimization process and corresponds

to the most energy-efficient stable walking orbit for the given walking speed and initial conditions.

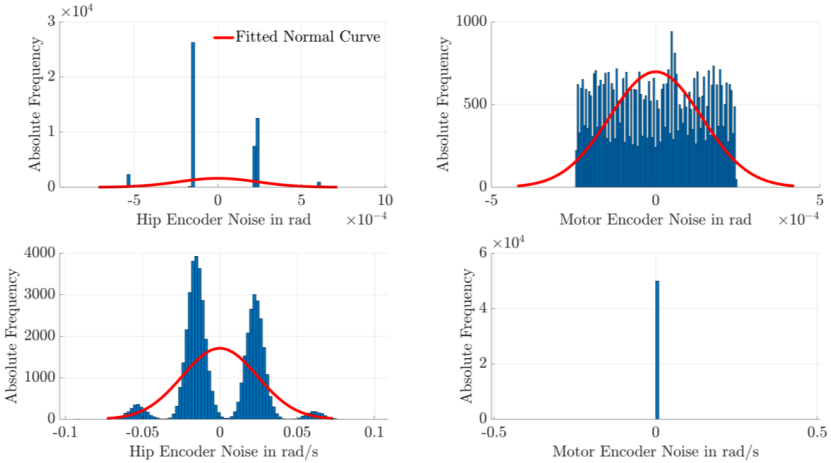

Figure 4: Histograms and corresponding fitted normal curves for angles (above) and velocities (below) measured by the hip and motor encoders

6. Results.

In the following results, the closed-loop system, illustrated in Figure 3, is tested against the performance of the *Ground Truth*. Moreover, the performance of the SEKF for the closed-loop system is compared against the traditional EKF introduced in Section 5.5. Firstly, the measurement covariance is set to the values evaluated from the analysis of the actual encoder measurements with the process covariance and initial error covariance parameters introduced in Section 5.4 being used. The performance of both EKF and SEKF for this case is extremely precise wherein the stable and periodic bipedal walking of the Ground Truth is almost perfectly recreated. Such precision should be expected since the evaluated measurement noise itself is quite minimal. However, in the physical walking experiments with the actual prototype, it was observed that the measurement noise plays a more significant role, wherein as the result of its introduction, such strong vibrations are induced within the mechanical system that the experiment can't be continued further. Some possible reasons for this might be the higher complexity of the actual prototype containing a lot of physical and electric couplings, the non-gaussian and colored noise behavior of the measurements, and electromagnetic interferences among the different electric components. Hence, the filter performance is inspected for

artificially augmented measurement noises. To that end, the sensor corruption values are randomly set to significantly higher values such that

$$\sigma^2 = \{0.005 \quad 0.005 \quad 0.005 \quad 0.005 \quad 0.005 \quad 0.02 \quad 0.02 \quad 0.02 \quad 0.02 \quad 0.02\}$$

When these noise parameters are introduced, the closed-loop system without any filter becomes unstable after the first walking step. $\boldsymbol{Q}_k$ and $\boldsymbol{P}_0$ are kept the same, and a grid search is performed in a relatively small and fine grid to find the best $\boldsymbol{R}_k$, for which the control error is the lowest. Figure 5 illustrates the obtained joint angles $\boldsymbol{q}_J$ for the closed-loop system with SEKF and EKF; and the Ground Truth. Figure 6 illustrates the phase orbits obtained from the closed-loop systems corresponding to the knee angle of the stance leg $q_{\mathrm{K,St}}$. It can be seen clearly, that the qualitative deviations of the EKF, especially after each impact are significantly higher than the SEKF, implying better post-impact state-estimations with the SEKF. Furthermore, the orbits obtained with the SEKF tend to stay closer to the ideal stable limit cycle of the Ground Truth, while the orbits obtained with the EKF show significantly larger deviations, increasing the probability of escaping into unstable regimes for higher measurement or process noise conditions. Hence, the superior performance of the SEKF, especially post-impact, can be concluded. Figure 7 illustrates the comparison between the noisy measurements for the virtual leg angle and the stance hip angle and their corresponding estimations from the SEKF, showcasing the effective measurement suppression achieved by the SEKF. Naturally, the filter convergence and estimation can be further improved by tuning $\boldsymbol{Q}_k$ and $\boldsymbol{P}_0$. The tuning process for SEKF on the actual prototype would be different, owing to the much higher system complexity and the resultant increased model deviations.

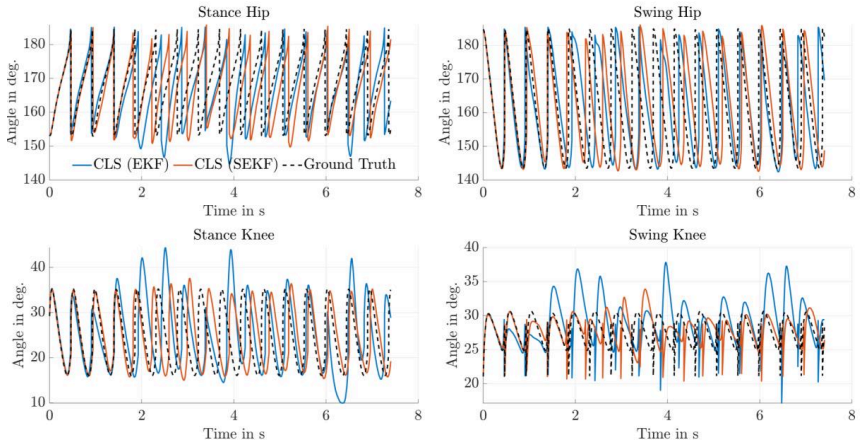

Figure 5: Joint Angles for Closed-Loop with SEKF (solid red), Closed-Loop with EKF (solid-blue) in comparison to Ground Truth (dashed black)

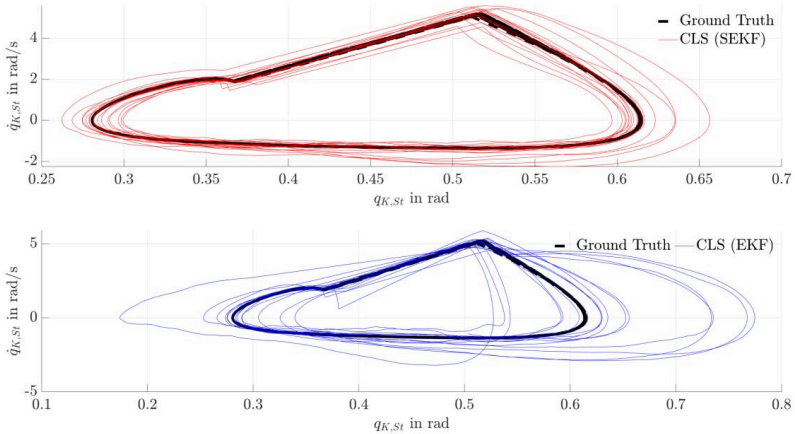

Figure 6: Phase Plots for Stance Knee Angle for Closed-Loop with SEKF (above) and Closed-Loop with EKF (below)

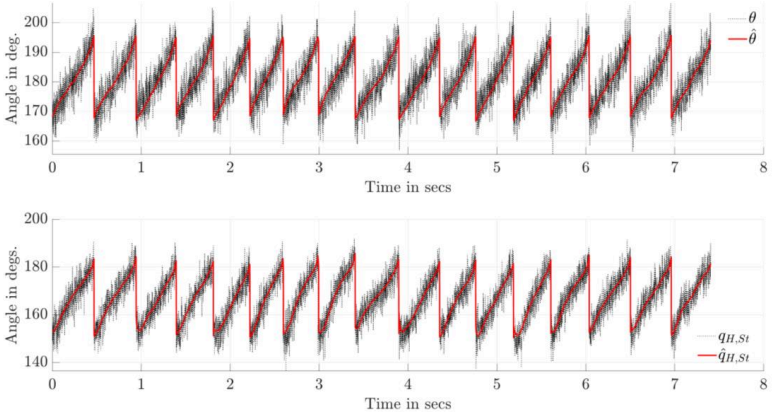

Figure 7: Noisy Measurements (dotted black) and their corresponding estimations (solid red) from the SEKF for the closed-loop system under augmented measurement noise

7. Conclusions and Future Outlook

In this study, the primary implementation of a Salted Extended Kalman Filter (SEKF) for the hybrid dynamic walking of a Bipedal Robot with point feet has been presented. The

performance of the SEKF was investigated for a real-time simulation framework to check the feasibility of deploying such a filter on a bipedal robot prototype and to examine the real-time abilities of the filter. The performance of the closed-loop system with the SEKF was investigated for two different cases of measurement noises: the first corresponding to the actual measurement noises evaluated from the motor encoders on the prototype and the second corresponding to augmented measurement noises to capture the effects of encoder measurements observed in previous walking experiments with the prototype. For both the cases, the SEKF is able to estimate states across discrete impact events reliably and facilitate the feedback controller in generating stable walking gaits while suppressing measurement noise, and furthermore shows superior performance compared to a traditional EKF. Since all simulations were performed in real-time, the real-time capability of the SEKF is also proven.

Within the scope of the simulation framework itself, there is scope for improvement in filter performance via extensive parameter tuning. For the deployment of the SEKF on the prototype, the process noise parameter would be more critical given the increased deviations between the actual prototype and the reduced model used for state propagation in the filter. The prototype is additionally equipped with analog strain gauges at the point feet to detect contact with the ground. Hence, for the prototype, the transition over the impact event is triggered based on not just the foot position conditions, but also the strain gauge measurement, which also possesses significant noise, suppressed currently using a moving average filter. Therefore, the observed state vector of the SEKF can be extended to include the strain gauge contact, and the measurements from the strain gauge can be fused within the filter as well. Through this, the strain gauge state can be estimated and the foot contact detection itself be made more robust. Ultimately, the performance of the SEKF needs to be compared with that of the low-pass filtering, which is also the current solution that has been implemented for the prototype. As explained in Section 1, the use of IMUs may also be sensible for the prototype, since they can be used to propagate the states and, in the process, help circumvent the use of the complex dynamic model of the walker, and the group-affine of the resulting system can be taken advantage of, consequently leading to improved filter performance.

Acknowledgements

This work is financially supported by the German Research Foundation (DFG), grant 416912124.

References

[1] Westervelt, E. R., Grizzle, J. W., Chevallereau, C., Choi, J. H., Morris, B.: Feedback Control of Dynamic Bipedal Robot Locomotion. Boca Raton: CRC Press 2018.

[2] Grizzle, J. W., Hurst, J., Morris, B., Park, H.-W., Sreenath, K.: MABEL, a new robotic bipedal walker and runner. In: American Control Conference (ACC), St. Louis (MO) 2009, pp. 2030–2036.
[3] Negrello, F., et al.: WALK-MAN humanoid lower body design optimization for enhanced physical performance. In: IEEE International Conference on Robotics and Automation (ICRA), Stockholm 2016, pp. 1817–1824.
[4] Hobart, C. G., et al.: Achieving versatile energy efficiency with the WANDERER biped robot. IEEE Transactions on Robotics 36 (2020) 3 pp. 959–966.
[5] Luo, Y., Römer, U. J., Zentner, L., Fidlin, A.: Improving energy efficiency of a bipedal walker with optimized nonlinear elastic coupling. In: Lacarbonara, W., Balachandran, B., Leamy, M. J., Ma, J., Tenreiro Machado, J. A., Stepan, G. (Eds.): Advances in Nonlinear Dynamics. Cham: Springer 2022, pp. 253–262.
[6] Luo, Y., Arbogast, P., Römer, U. J., et al.: Study on bipedal running on compliant ground using hybrid zero dynamics controller. Multibody System Dynamics (2025), online first.
[7] Aizerman, M., Gantmakher, F.: On the stability of periodic motions. Journal of Applied Mathematics and Mechanics 22 (1958) 6 pp. 1065–1078.
[8] Kong, N. J., Payne, J. J., Council, G., Johnson, A. M.: The salted Kalman filter: Kalman filtering on hybrid dynamical systems. Automatica 131 (2021) pp. 109752.
[9] Bloesch, M., et al.: State estimation for legged robots: Consistent fusion of leg kinematics and IMU. In: Roy, N., Newman, P., Srinivasa, S. (Eds.): Robotics. Cambridge (MA): MIT Press 2013, pp. 17–24.
[10] Bledt, G., Powell, M. J., Katz, B., Di Carlo, J., Wensing, P. M., Kim, S.: MIT Cheetah 3: Design and control of a robust, dynamic quadruped robot. In: IEEE/RSJ International Conference on Intelligent Robots and Systems (IROS), Madrid 2018, pp. 2245–2252.
[11] Hartley, R., Ghaffari, M., Eustice, R. M., Grizzle, J. W.: Contact-aided invariant extended Kalman filtering for robot state estimation. The International Journal of Robotics Research 39 (2020) 4 pp. 402–430.
[12] Barrau, A., Bonnabel, S.: Invariant Kalman filtering. Annual Review of Control, Robotics, and Autonomous Systems 1 (2018) 1 pp. 237–257.
[13] Payne, J. J., Kong, N. J., Johnson, A. M.: The uncertainty aware salted Kalman filter: State estimation for hybrid systems with uncertain guards. In: IEEE/RSJ International Conference on Intelligent Robots and Systems (IROS), 2022, pp. 8821–8828.
[14] Gao, Y., Yuan, C., Gu, Y.: Invariant extended Kalman filtering for hybrid models of bipedal robot walking. IFAC-PapersOnLine 54 (2021) 20 pp. 290–297.
[15] Mazumdar, A., et al.: Synthetic fiber capstan drives for highly efficient, torque controlled, robotic applications. IEEE Robotics and Automation Letters 2 (2017) 2 pp. 554–561.
[16] Mukherjee, A., Luo, Y., Zirkel, M., Gerlach, E., Zentner, L., Fidlin, A.: Identification of energy dissipation models in the drivetrain of an energy efficient bipedal robot. In: Proceedings of the 16th International Conference on Vibration Problems, in press.
[17] Wendel, J. (Ed.): Integrierte Navigationssysteme: Sensordatenfusion, GPS und Inertiale Navigation. 2nd ed. München: De Gruyter 2011.
[18] Kong, N. J., Payne, J. J., Zhu, J., Johnson, A. M.: Saltation matrices: The essential tool for linearizing hybrid dynamical systems. Proceedings of the IEEE 112 (2024) 6 pp. 585–608.
[19] Akhlaghi, S., Zhou, N., Huang, Z.: Adaptive adjustment of noise covariance in Kalman filter for dynamic state estimation. arXiv preprint 1702.00884 (2017).